

Vehicular Classification Based on Vibration Caused by Uncontrolled Traffic Using Fibre Optic Sensor

Awodu Onuora*

Co-Authors: Ukagwu Kelechi**, Okuonghae Timothy* and Azi S.O*.

*Department of Physics, Faculty of Physical Sciences, University of Benin, Nigeria

**Department of Physics, Mountain Top University, Nigeria

Abstract: Fibre optic vibration sensor (FOVS) converts vibration signal to light signal. Due to its prominent features, distributed fibre optic vibration sensor is preferred to conventional methods. Interest in FOVS has greatly increased over the years in structural health monitoring and vehicular traffic, hence the need to embark on this study. Distributed FOS is employed to measure the frequency of vibration caused by uncontrolled vehicular movement at Oluku By-Pass Bridge. Φ -OTDR is used to obtain millisecond snapshots of the stochastic signal arising thereof. A video shot was also recorded to match the exact timing of each excitation.

Traces obtained show several frequency peaks at various corresponding backscatter level for high and low vehicular traffic. Sampled data analyzed with Fiberizer Cloud software indicates high attenuation contribute to low total loss and low attenuation lead to high total loss. Spectral analyses of the data at low and high traffic for the stochastic signal. The corresponding frequency peaks were calculated and the results used to classify vehicles at low and high speed. The FWHM obtained with double Gaussian model for differential trace shows that high traffic gives sharp peaks with standard deviation less than 0.6 and above 0.6 for low traffic. The analyses identified peaks above 4.0×10^{-3} for traces with trucks and cars at high speed, while peaks less than 4.0×10^{-3} were obtained for traces with cars.

1.0 INTRODUCTION

Vibration is a common phenomenon in nature. A sensing device that converts vibration into electrical signals is called as vibration sensor [1]. In recent years, vibration sensing technology has improved significantly in structural health monitoring, equipment manufacture and maintenance [2]. The most common conventional vibration sensors used include; piezo-electric, strain gauge, piezo-resistive accelerometers.

The undersized monitoring range and high maintenance cost of conventional sensors led to demands for improved modern vibration monitoring and analysis. This study is focused on vibration measurement caused by vehicular traffic. Road monitoring is a vital issue in developing countries with insufficient road construction and epileptic maintenance system in the country. Unlike conventional method of sensing, optical fibers have gained interest due to its wide range of applications in the past decades, hence its use as fibre optic sensor. Generally, the operating principle of a fiber-optic vibration sensor is based on the modulation of the light characteristics. Such as light intensity, phase and polarization, when the fibre excited by external perturbation. The distributed fibre optic vibration sensing (DOVS) technology is a type of FOS that has gained popularity in road and railway monitoring over the years [3]. Its precise measurement of weight-in-motion has long been a major objective of highway engineers in road construction. Several WIM techniques have been developed for measuring vehicular traffic on highway in the past decades. The data obtained aids civil engineers in road construction, maintenance and monitoring as well as highway safety assessment and improvement [4].

Fibre optics has gained popularity in present day due to its prominent use in sensor technology as an addition to its major applications in communication networks [5]. Recently, FOS has gained increased popularity and market acceptance. In comparison to conventional sensors they offer a number of distinct advantages which makes them unique for certain types of applications, mainly areas where conventional sensors are difficult to function [6].

Applications of FOS are as follows; it is used to measure physical properties such as strain, temperature, pressure, and other quantities by modifying the fibre to suit the desired measurement in other to modulate light intensity, phase, polarization, wavelength and other parameters with an fibre optic cable [7]. [8] reviewed some fibre optic sensor topology and techniques to determine their suitability for various applications as stated in Table 1

Table 1: Different classifications of FOS

Working Principle [9]	Spatial Positioning [8]	Measured Parameters [7,10]
Intensity-modulated sensors: Detection through light power	Point sensors: Discrete points, different channels for each measurement	Physical sensors: Temp., strain, pressure, force, speed and displacement (amplitude) sensors, Acoustic and vibration sensors, humidity etc.
Phase-modulated (interferometric) sensors: Detection using the phase of the light beam	Distributed: Measurement is determined along a path, surface, or volume	Chemical sensors: pH content, gas sensors, liquid level, spectroscopic study, etc.
Polarimetric sensors: Detection of changes in the state of polarization of the light	Quasi-distributed: Variable measured at discrete points along an optical link	Biosensors: DNA, blood flow, glucose sensors etc.
Spectrometric sensors: Detection of changes in the wavelength change of the light	Integrated: Measurement integrated along an optical link giving a single value output	Chemical and Biosensors

It can be used in structural health monitoring of buildings and bridges, tunnels, dams, heritage structures, night vision camera, electronic security systems, partial discharge detection and measuring wheel loads of vehicles.

Precise measurement and monitoring of vibration is vital in detecting abnormal events and pre-warning of infrastructure damage [11]. [12] reviewed the trend of modern sensors; it was discovered that in practice, the fibre optics used as an intrinsic sensor for vibration proved difficult when separating the various changes encountered from other physical quantities. It was rather used as a medium of transmission of light and other sensitive device to detect changes of the measured physical quantity and the light parameter modulated by sensitive components.

The trend in fibre optics sensing technology highlights the development of optical interferometry and modulation techniques [10]. The fibre optics classification based on the working principle/modulation was reviewed, which requires an external perturbation as light propagates along the fibre as stated in Table 1.

It can also be stated that bridge structures rely on the mass and solidity of the materials used and its ability to resist external pressure despite their incapable to adapt to the dynamic change of the environment. This

results to structural failure of the bridge when considering the structural health [13]. Thorough investigation in distributed fibre optic vibration sensors has evolved and its relevance cannot be over emphasized in determining the optical parameters such as light intensity, phase and polarization changes when external perturbation is applied on the sensing fibre [14].

[15] designed and measured the instantaneous amplitude and frequency of vibration of a vibrating medium over a small-localized surface area by means of a fibre optic probe. The data obtained from his technique had restrictions but conforms to the conventional method in measuring the instantaneous amplitude and frequency but limited to only the first order vibrations, since the research is for a very small region.

As stated in section 1.5, several distributed FOVS measurement are used to measure various physical parameters along the fibre as shown in Figure 2.9

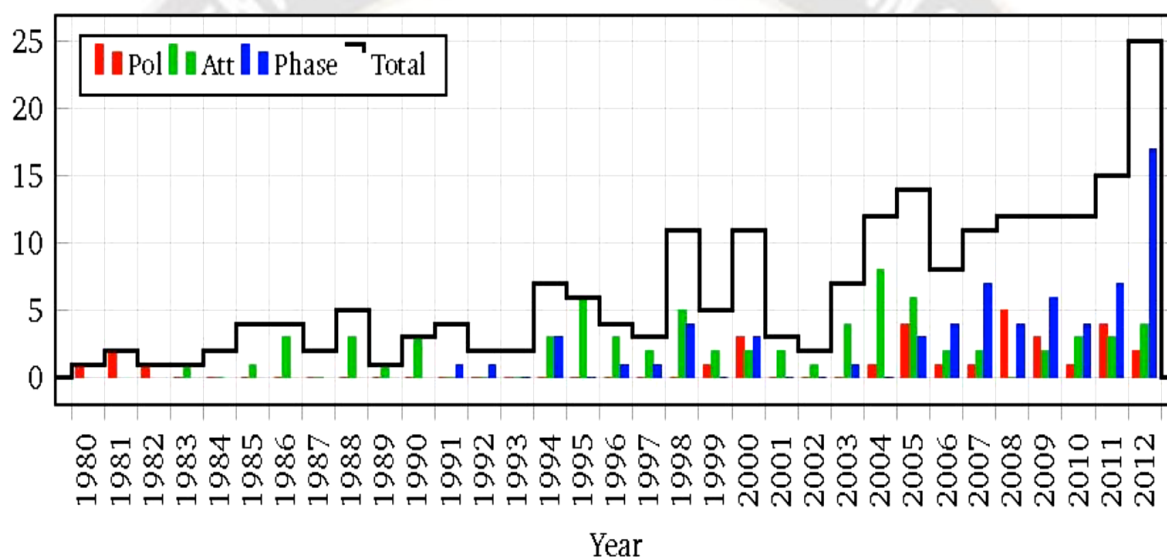


Figure 1.1: Peer review articles on Rayleigh-Based Distributed FOS [16]

A Comparative review on the sensing mechanism for polarization, phase and attenuation based measurement relating to backscatter-based distributed FOS was carried out. It was observed that a high number of peer review articles relating to Rayleigh based distributed fibre optic sensors use phased based FOS as shown in Figure 1.1. Red, green and blue bar represent peer reviews on polarization, attenuation, and phase based distributed FOS respectively. The black line represents total number of peer review articles per year [16].

Though, polarization based measurement is barely used as stated in Figure 2.9, literature exist in that study area. [17] measured vibration effect based on spectrum analysis using a polarized OTDR. The data analyzed showed variation in the signal at different frequencies along the fibre cable. FOS can also be used in for gas pipeline leakage monitoring in an oil and gas industry with the help of a Sagnac/Mach-Zehnder Interferometer configuration [18]. The design was used for a fibre length range of 1.5-9.5km, with the light intensity reducing to -56dB for pipeline with leakage and without leakage and the results yielded a positive response, with the vibration system having a sensitivity of 0.57Hz/m.

Due to the growing interest in structural health monitoring, the awareness of the dynamic characteristics of a bridge structure cannot be over-emphasized. The defects are as a result of heavy duty objects and wind constantly plying the bridge at certain momentum, which results to the deformation of the modal

characteristics of the bridge structure. Hence the need for continuous monitoring of the bridge structure, as significant data obtained will contribute to a stable and safe operation of the bridge and can be used for the calibration of a structural numerical model [3].

[19] reviewed fibre optics sensing technologies for industrial applications at National Engineering laboratory for Fibre Optics Sensing Technology (NEL-FOST). They further described the various applications of FOS for structural health monitoring, high-speed railway monitoring and transformer temperature monitoring, which can either be point, distributed, quasi-distributed sensors as described in Table 1.2 [20]

Table 1.2: Fibre Optic Vibration Sensor Applications

CLASSIFICATION	MEASUREMENT TECHNIQUE	MEASUREMENT PARAMETERS	WORKING PRINCIPLE	MEASURE TYPE	ADVANTAGES
Point Sensor	Interferometric : Fabry-Perot	Temperature, strain, pressure, displacement, refractive index etc.	Intensity/ phase	Intrinsic/ Extrinsic	High sensitivity but complex interrogation, limited multiplexing capacity, WDM is difficult.
	Mach-Zehnder	Temperature, strain, pressure, displacement, refractive index, etc.	Intensity/ phase	Intrinsic/ Extrinsic	Compactness and high efficiency combined with ease of fabrication, but complex interrogation
	Michelson	Temperature, strain, pressure, displacement, refractive index, etc.	Intensity/ phase	Intrinsic/ Extrinsic	High accuracy, compactness, good multiplexing capability, complex interrogation.
Quasi-distributed	Interferometric : Sagnac	Optical gyroscopes, strain, pressure, twist	Intensity/ phase	Intrinsic	Simple and easy to fabricate but suffer from the significant temperature strain cross-sensitivity.
	Fibre Bragg Gratings	Temperature, strain, pressure, can be configured to measure displacement, acceleration, etc.	Wavelength	Intrinsic	Excellent WDM capability, advantages of wavelength encoding but disadvantages of cross-sensitivity between strain and Temp.
Distributed	Rayleigh Scattering	Temperature, strain	Intensity (OTDR)	Intrinsic	High strain/temperature resolution and good spatial resolution, but limited length; Temp. compensation required
	Raman scattering	Temperature	Intensity (OTDR)	Intrinsic	Advantageous for temperature sensing only,

					since no particular packaging needed to make sensing fibre strain free
	Brillouin Scattering	Temperature, strain	Intensity (BOTDR)	Intrinsic	Advantage of relatively stronger signal but synchronization of two laser sources at the opposite ends of the fibre is required

In developing countries like Nigeria, road monitoring and maintenance is a major issue for easy movement. Several FOS techniques is considered to identify a lasting solution to road degradation. Some factors that affect the accuracy of FOS vibration measurement caused by vehicular movement include; installation of the sensor on the road-side, nonlinearity and inertia of the sensor, inertial force of the vibrating vehicles, thermal effect and extremely short time of the load on the sensor [21]. Techniques are still being exploited to analyze the vibration caused by vehicular movement. [4] measured wheel loads of vehicles using a fibre optics sensing technique. A fibre having two concentric light guiding regions of separate optical path with the potential to measure backscatter resulting from bending at distributed points on a single-mode fibre cable. The results showed that load applied on a fibre changes the light intensity along the fibre core. Also a correlation of time delay between the inner and outer core light pulses and the distance of the applied load as measured from the output end of the fibre was established.

Over the years, distributed vibration sensor has evolved in monitoring traffic on highways [22], although there has been little or no reports of actual implementation with distributed FOVS. However, applications arise in this area on monitoring of vehicular traffic and their speed, as well as weight-in-motion (WIM); that is, estimating in real-time vehicle classification based on their axle type and category of vehicles [23] as described by [24]. Most point sensors are used for analyzing vehicular traffic on highway and bridge [25].

Vehicular vibration was used to classify vehicles based on their axle type. An embedded fibre optic cable was used as a distributed sensor to obtain vibration resulting from controlled vehicular traffic [24]. A multi-step classifier was designed to categorize vehicles into different classes. The sampled data was used to estimate vehicles based on their axle configuration and vehicle categories. To achieve this, empirical mode decomposition (EMD) based method was used to reconstruct the signals, extract the features and apply an algorithm to obtain the axle configuration, vehicular speed and the spectra of each vehicle. Though this distributed optical vibration sensing technique is rather complex, an overall accuracy of 89% was achieved, with the test results showing good performance of this classification system.

Unlike previous literatures, most intensity based sensor are characterized using a Fibre Bragg Grating but this study has shown that a fibre cable and Φ -OTDR can be used to measure vibration caused by vehicular movements at Oluku by analyzing the fluctuation in light intensity within the cable.

1.1 OPTICAL TIME DOMAIN REFLECTOMETER

In recent years, fibre optics applications have extended beyond communication. It is employed in optical networking and fibre optic sensor technologies. Spatial positioning in fibre sensors are very important aspect in fibre optic sensor as a fibre cable can behave like hundreds or thousands of sensors spread along it. To this end, the response to test signal of a FOS has provide information not only about the value of the

measured quantity but also about the created response location, with respect to time [26]. The most common solutions of these systems are based on the reflectometry principle. The spatial resolution can be obtained spans from micrometers for short sensor lengths to tens of kilometers for long range sensors [27].

OTDR is an optoelectronic device that launches a series of probe pulses into an optical fibre and detects the optical signals returning to the initiation end. It has demonstrated over the years to be widely used for locating fibre breaks and locate abnormalities within the fibre cable over a distance, and determines the amount of signal loss at any point in the fibre. This can be stored for future reference for comparison and analysis. It detects the effects of perturbations at a specific location, which has resulted to several OTDR design that respond to phase changes of the radiation (light) to enhance coherent effects [28].

The OTDR consists of a high power laser transmitter that transmits a pulse of light through the fibre core; an optical sensor, which measures the backscattered/reflected lights through a coupler/splitter in the OTDR front end; a display and controller sections as shown in Figure 2.1

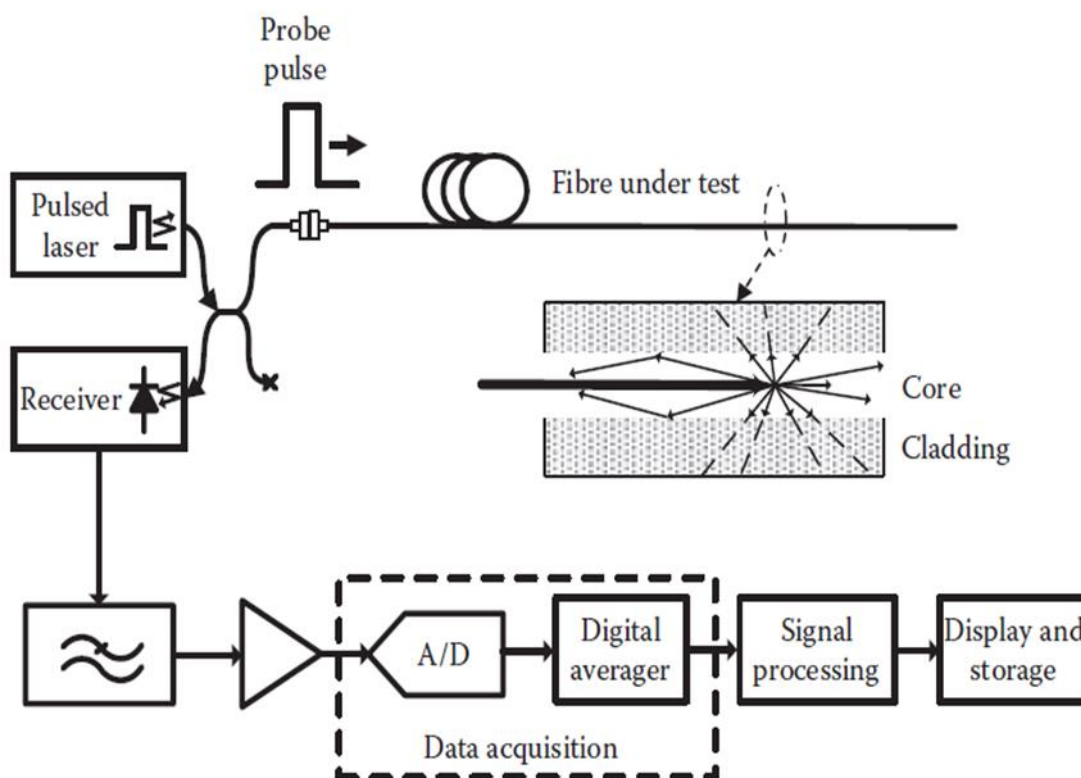


Figure 1.2: Schematic diagram of an OTDR [23]

The Rayleigh backscattered event is collected by the photodetector through directional coupler-splitter and produces an event trace. The OTDR identifies the presence and position of external perturbations which affect the light intensity of the light returned from the fibre as shown in Figure 2.1.

In order to avoid superposition of the backscattered signal, a single pulse is sent into the fibre at a time. Hence, the repetition rate of optical pulse is limited by the fibre length and time lag between the pulses is given by [29];

$$\tau = \frac{2L}{v_g} \tag{1}$$

where L is the distance from the input end and V_g is the group velocity of the propagating light in the fibre. In the configuration of an OTDR, the spatial resolution and dynamic range are the most important parameters that characterize its performance. The spatial resolution Δz , which is the minimum resolvable distance is determined by the width of the launched pulse as described in equation (2)

$$\Delta z = \frac{T_p V_g}{2} \quad (2)$$

where T_p is the pulse width of the incident light

When attenuation is constant for both direction of propagation, the backscattered power (P_{bs}), can be calculated using equation (3)

$$P_{bs} = \frac{F a_s T_p V_g P_o e^{-2\alpha L}}{2} \quad (3)$$

where a_s is the Rayleigh scattering coefficient, α is fibre attenuation coefficient, F is the capture coefficient and P_o is the input power.

The dynamic range is the difference between the initial backscatter power level and the noise level of a measurement time. It can be increased by either enhancing the backscatter power or decrease the noise level. The backscattered power is proportional to the product of pulse width T_p and input power P_o .

However for an OTDR, a pulse with very high peak power is not desired because it will cause a nonlinear effect within the fibre. Thus, dynamic range solely depends on the pulse width. Increasing the dynamic range requires the longer pulses which would decrease the spatial resolution as defined in equation (2). This trade-off between the dynamic range and spatial resolution represents the fundamental limit of the OTDR system. For this study, OTDR with a short pulse width was used to measure vibration resulting from uncontrolled vehicular traffic. The backscattered power in equation (3) was used to obtain a trace with both parameters considered to obtain the precise measurement.

Therefore, the backscatter factor $\eta(z)$ is given by

$$\eta(z) = \frac{V_g}{2} \alpha_s(z) \cdot F(z) \quad (4)$$

They are widely used in all areas of a fibre system's life, from construction to maintenance to fault locating and restoration. It is also widely used in structural health monitoring and to locate fibre breaks or pipeline leakages and other abnormalities (such as scattering, bends etc.) in fibre optic links and networks. It is used to measure splice loss-both fusion and mechanical splices; during installation, construction, and restoration operations. It measures overall (end-to-end) loss for system acceptance and commissioning; and for incoming inspection and verification of specifications on fibre reels. Loss associated with intensity and phase modulated, polarimetric and spectrometric sensors can also be measured.

1.2 ANALYSIS OF RAYLEIGH SCATTERING

As light propagates through a fibre core, the power decreases constantly due to scattering. As stated in chapter one, Rayleigh scattering is created due to excitation and variation in the optical properties of the fibre. The intrinsic loss of the fibre core from Rayleigh scattering is expressed mathematically as [30]:

$$\alpha_s = \frac{c}{\lambda^4} \quad (5)$$

where constant, c is the range 0.7-0.9 (dB/km) μm^4 , depending on the constituents of the fibre core.

When light is launched into the fibre, the electromagnetic (EM) field readjusts the fibre characteristics of the disjointed molecular clouds to respond equally on a small spatial scale covering a small fraction of the

wavelength of the EM field. This dual response to an EM field will result in macroscopic polarization that is proportional to the external electric field E , that is;

$$P = \epsilon_0 \dot{Y}E \tag{6}$$

where ϵ_0 is the vacuum permittivity and \dot{Y} is the material status dependent quantity symbolizing the dual response. Also, \dot{Y} includes a random fluctuation part $\Delta\epsilon(t,z)$. Therefore a change in the polarization-induced light emission in all directions is caused by the variable dielectric parameter $\Delta\epsilon$.

Some of the Rayleigh scattered light is recaptured by the waveguide and guided in the backward direction, towards the source. For non-conducting material, Maxwell's equation is given by;

$$\nabla \times \vec{E} = -\frac{\partial \vec{B}}{\partial t}; \nabla \times \vec{H} = \frac{\partial \vec{D}}{\partial t}; \nabla \times \vec{D} = 0; \nabla \cdot \vec{B} = 0 \tag{7}$$

where \vec{E} and \vec{H} are electric and magnetic fields vector respectively. \vec{D} and \vec{B} are electric and magnetic flux densities. The constitutive relationship between flux density and the field vector is given by;

$$\vec{D} = \epsilon_0(1 + \dot{Y})\vec{E} = (\epsilon + \Delta\epsilon)\vec{E} \text{ and } \vec{B} = \mu_0\vec{H} + \vec{M} \tag{8}$$

where ϵ is a constant and $\Delta\epsilon$ describes the Rayleigh scattering, which is the variation of the permittivity of the fibre core as a function of time and distance. μ_0 is the vacuum permeability and M is the induced magnetic polarization, which is equal to 0 for a non-magnetic medium (fibre optics).

Combining equations (7) and (8), the wave equation of electric field is obtained.

$$\mu_0\epsilon = \underbrace{\frac{\partial^2 \vec{E}}{\partial t^2} - \nabla^2 \vec{E}}_{\text{Ordinary Coherent Propagation Process}} - \underbrace{\nabla[\vec{E} \cdot \nabla \ln(\epsilon + \Delta\epsilon)]}_{\text{Random Spontaneous Scattering caused by Rayleigh scattering}} + \underbrace{\mu_0 \frac{\partial^2(\Delta\epsilon \vec{E})}{\partial t^2}}_{\text{Random Spontaneous Scattering caused by Rayleigh scattering}} = 0 \tag{9}$$

It is safe to assume that $\Delta\epsilon$ is time dependent by $-i\omega$. Therefore, equation (9) can be rewritten as;

$$\nabla^2 \vec{E} + \nabla[\vec{E} \cdot \nabla \ln(\epsilon + \Delta\epsilon)] + \mu_0\epsilon\omega^2 \left(1 + \frac{\Delta\epsilon}{\epsilon}\right) \vec{E} = 0 \tag{10}$$

For fibre optics, the lateral dependence of the electric field can be ignored. Hence, only the longitudinal dependence on z -direction can be considered. This gives a scalar equation of;

$$\frac{\partial^2 \vec{E}}{\partial z^2} + \beta^2 \left(1 + \frac{\Delta\epsilon_z}{\epsilon}\right) \vec{E} = 0 \tag{11}$$

where $\beta = \omega\sqrt{\mu_0\epsilon}$ is the propagation constant. One can propose a solution comprising of forward (first term) and backward (second term) propagation of a travelling wave shown in equation (12)

$$\vec{E} = E_0 e^{i\beta z} + \Psi_{(z,\beta)} e^{i\beta z} \tag{12}$$

Substituting equation (12) into (11) and applying the slow amplitude variation (that is, $\frac{\partial^2 \Psi}{\partial z^2} \cong 0$), we have;

$$2i\beta \frac{\partial \Psi}{\partial z} - \beta^2 \frac{\Delta\epsilon(z)}{\epsilon_0} E_0 e^{2i\beta z} - \beta^2 \frac{\Delta\epsilon(z)}{\epsilon_0} \Psi = 0 \tag{13}$$

For weak Rayleigh scattering over short distances,

$$\Psi_{(z,\beta)} \ll E_0 \tag{14}$$

An approximation solution for Rayleigh backscattered light caused by random spatial variation of the permittivity can be assumed as;

$$\Psi_{(z,\beta)} - \Psi_{(0,\beta)} \approx \frac{\beta E_o}{2i} \int_0^z \frac{\Delta \epsilon(\zeta)}{\epsilon_o} e^{2i\beta\zeta} \partial\zeta \quad (15)$$

where $\Psi_{(0,\beta)}$ is the end-face reflection signal

Since scattering (Rayleigh scattering and material absorption) is the basic mechanism for fibre loss, the total attenuation coefficient α is given by;

$$\alpha = \alpha_s + \alpha_a \quad (16)$$

where α is total attenuation coefficient, α_s is Rayleigh scattering and α_a is material absorption

From this work, it is safe to deduce that Rayleigh backscatter power attributes to majority of the fibre loss. Hence, the backscatter power can be estimated if certain parameters are known. Due to the attenuation loss, the input power will decrease exponentially as a function of the propagating distance (z) as shown in equation (17) [29, 30].

$$P_{(z)} = P_o e^{-i\alpha z} \quad (17)$$

where P_o is incident light power and $P_{(z)}$ is the transmitted power at distance (z)

Since attenuation coefficient α is expressed in dB/km, equation (17) can be rewritten as;

$$P_{(z)} = P_o e^{-\frac{i\alpha_{dB}z}{10}} \quad (18)$$

Therefore, $\alpha_{dB} = \frac{10}{\ln 10} \cdot \alpha \approx 4.34\alpha$ (15)

1.3 LIGHT INTENSITY IN A FIBRE OPTIC CABLE

In order to achieve a valid result, the light intensity propagation in a multi-mode fibre was derived from the well-known Helmholtz equation originating from Maxwell's equation to deduce the effect of forced vibration on the cable and hence the total light intensity after perturbation.

$$\nabla^2 \vec{E}(r) + K^2 \vec{E}(r) = 0 \quad (15)$$

This is regarded as Helmholtz Equation

Light in fibre optics propagation in cylindrical coordinates, hence we have [31];

$$\frac{d^2 E(r)}{dr^2} + \frac{1}{r} \frac{dE(r)}{dr} + \frac{1}{r^2} \frac{d^2 E(r)}{d\theta^2} + \frac{d^2 E(r)}{dz^2} + K^2 E(r) = 0 \quad (16)$$

Equation (3.2) can be rewritten as

$$\theta Z \frac{d^2 R}{dr^2} + \frac{1}{r} \theta Z \frac{dR}{dr} + \frac{1}{r^2} R Z \frac{d^2 E}{d\theta^2} + R \theta \frac{d^2 E}{dz^2} + K^2 = 0 \quad (17)$$

Dividing through by $R\theta Z$ and differentiating, we have

$$\frac{d^2 R}{dr^2} + \frac{1}{r} \frac{dR}{dr} + \left(K^2 - \beta^2 - \frac{n^2}{r^2} \right) R = 0 \quad (18)$$

Further calculations give the general form of the Bessel's equation, which has the solution;

$$R = AJ_n(r\gamma) + BJ_{-n}(r\gamma) \quad (19)$$

As r tends to infinity, the second term of the Bessel's equation tends to infinity. That is,

$BJ_{-n}(r\gamma) \rightarrow 0$, hence, we have

$$R = A J_n(r\gamma) \cos n\theta e^{-i\beta z} \quad (20)$$

Therefore, the electric and magnetic fields becomes

$$E = A_m J_{n_m}(u_m r) \cos n_m \theta e^{-i\beta_m z} \quad (21)$$

$$B = A_l J_{n_l}(u_l r) \cos n_l \theta e^{-i\beta_l z} \quad (22)$$

The light intensity is given by

$$I = \frac{\epsilon_0 C}{2} A_m A_l J_{n_m}(u_m r) J_{n_l}(u_l r) \cos n_m \theta \cos n_l \theta e^{-\beta_m z} \quad (23)$$

As m and l take several values, we have

$$I = \frac{\epsilon_0 C}{2} \sum_{m=0}^N \sum_{l=0}^N A_m A_l J_{n_m}(u_m r) J_{n_l}(u_l r) \cos n_m \theta \cos n_l \theta e^{-\beta_{ml} z} \quad (24)$$

This is regarded as light intensity in fibre cable.

The light intensity of a single-mode (SM) or multi-mode (MM) fibre is dependent on the phase shift as the light intensity in a fibre cable is perturbed by an external factor (vehicular movement). SMF is mainly used for long haul, which implies that the phase shift is required to be minimal but for a MMF, it is obvious as shown in the equation (25).

$$I = \frac{\epsilon_0 C}{2} \sum_{m=0}^N \sum_{l=0}^N A_m A_l J_{n_m}(u_m r) J_{n_l}(u_l r) \cos n_m \theta \cos n_l \theta e^{[-i(\Delta\beta_{ml} z - \Delta\phi_{ml})]} \quad (25)$$

where $e^{[-i(\Delta\beta_{ml} z)]}$ is change in propagation const. along the fibre as it experience perturbation
 $e^{[-i(\Delta\phi_{ml})]}$ is change in phase in the multi-mode fibre

Recall from equations (11) and (12), β is light propagating the fibre core in forward and backward direction. Therefore, detecting the changes of output light intensity, the light intensity inside a multi-mode fibre can be represented as [32];

$$I_{(r,\theta)} = \frac{1}{2} Y \sum_{m=0}^M \sum_{N=0}^N A_m A_N J_{n_m}(U_m r) J_{n_l}(U_l r) \cdot \cos(n_m \theta) \cos(n_l \theta) e^{[-i(\Delta\beta_{ml} z - \Delta\phi_{ml})]} \quad (26)$$

When forcing function F(t) is applied, equation can be rewritten as;

$$I_i = A_i \{1 + B_i [\cos \delta_i] - F(t) \theta_i \sin(\delta_i)\} \quad (27)$$

Therefore, change in light intensity resulting from an applied forcing function is given as

$$\Delta I_T = \left| \sum_{i=0}^N C_i \sin(\delta_i) \right| \left| \frac{dF(t)}{dt} \right| \quad (28)$$

As light propagates through the fibre cable, the intensity is altered due to cable perturbation. The pressure exerted on the cable caused by vehicular movement creates an impression on the fibre core as light travels through it. The change in light intensity caused by the forcing function (uncontrolled vehicular movement) is derived in equation (28). This attenuation is measured using OTDR in the form of backscattered resulting from the vehicular movement, $F(t)$ is calculated using equation (15). It is possible by determining the backscatter level resulting from the forcing function. As light incident on the impression caused by vehicle tyre, the OTDR measures the Rayleigh backscatter along the fibre cable as described in equation (18). This implies that vibration can affect light intensity in fibre optics, and the excitation caused by vehicular movement is explicitly derived in equation (28).

1.4 Rayleigh Scattering

As light pulse propagates through the fibre core, it interacts with some microscopic particles (silica glass) and is scattered in all directions. The elastic collision results in Rayleigh scattering. The total attenuation in a fibre is described in Figure 1

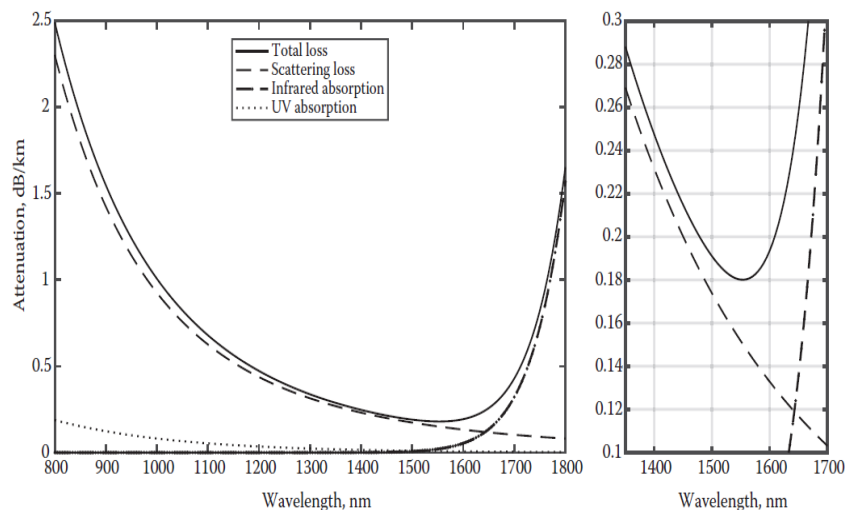


Figure 1.3: Rayleigh scattering in fibre optic cable [23]

The total loss indicates a minimum near at a wavelength of 1550 nm. The reduction in loss for increasing wavelength due to the UV absorption and Rayleigh scattering is annulled by the sharp increase in IR absorption. The energy of the scattered photons for Rayleigh scattering is the same as that of the incident photon; hence the wavelength is preserved in the scattering process. It also preserves the polarisation of the incident light: in silica, about 5% of the scattered light intensity occurs in the polarisation orthogonal to that of the incident light, whereas 95% remains in the original polarization [23].

OTDR measures the level of backscattering accurately, and uses it to detect small variations in the characteristics of fibre at any point along its length. This attenuation is caused by the reduction in the power level, due to the Rayleigh backscatter. Its loss provides an attenuation that is proportional to $\frac{1}{\lambda^4}$ throughout the visible and near-infrared spectra regions with a minimum of 0.2 and 0.3dB/km at a wavelength of 1550nm and 1310nm respectively. The backscatter power is a function of the Rayleigh scattering coefficient, fibre attenuation, capture coefficient, group velocity and input power as described in equation (19).

1.5 SPECTRAL ANALYSIS

The OTDR measures the variation in a fibre by either a single-ended and double-ended measurements. A single-ended measurement involves attaching an OTDR at one end of the fibre to serves as both a light source and obtains the backscatter trace, while a double-ended involves having a light source at one end of the fibre and an OTDR at the other end. For a single-ended measurement, the OTDR measures the backscatter as described in equation (19) and (20), caused by variation of the backscatter factor resulting from change in scattering loss. The trace obtained from this measurement is therefore abstruse [23].

Measured data obtained with an OTDR, especially with a single-ended measurement usually requires further analysis to analyze the spectra using a parametric model [33].

Parametric model is considered when there is information about the signal. Examples include Yule-Walker and Burg models. There are two main methods; auto-regression, which assumes the signal, can be modeled as the output of an autoregressive filter and subspace, which separates the signal into a signal subspace and noise subspace. Thereby exploiting the orthogonality between the two subspaces and allows a pseudospectrum to be formed, such that large peaks at narrowband components can appear. The PSD of a signal $y(t)$, is analyzed using an appropriate filter with transfer function $H(w)$ stated in equation [33].

$$H(w) = \frac{B(w)}{A(w)} \tag{21}$$

Where; $A(w) = 1 + a_1e^{-iw} + \dots + a_n e^{-inw}$ (22)

$$B(w) = 1 + a_1e^{-imw} + \dots + a_n e^{-imw}$$
 (23)

In time domain field, the above filter is expressed as

$$y(t) + \sum_{i=1}^m a_i y(t-i) = \sum_{j=0}^m b_j e(t-j), (b_0 = 1) \tag{24}$$

where $y(t)$ is signal; $\sum_{i=1}^m a_i y(t-i)$ is Auto-regression and $e(t-j)$ is white noise.

Condition $m = 0$ was used for an auto-regressive signal, AR(n); hence the expectation value gives;

$$r(k) + \sum_{i=1}^m a_i r(k-i) = \sum_{j=0}^m b_j E \left\{ e_{(t-j)} y_{(t-k)}^* \right\} \tag{25}$$

This gives rise to;

$$r(k) + \sum_{i=1}^n a_i r(k-i) = \sigma^2 \sum_{j=0}^m b_j h_{j-k}^* \tag{26}$$

For Auto-regressive signal (AR), m is equal 0 and $B(q) = 1$, equation (30) becomes;

$$r(0) + \sum_{i=1}^n a_i r(-i) = \sigma^2 \sum_{j=0}^0 b_j h_{j-k}^* = \sigma^2 \tag{27}$$

Therefore, for $H(q)$ to be causal, $h_l = 0$ for $l < 0$. This implied that for $k \geq m + 1$, equation (2.28) becomes;

$$r(k) + \sum_{i=1}^n a_i r(k-i) = 0 \quad \text{for } k > m \tag{28}$$

Substituting the appropriate coefficients, the result gives the matrix, with the first row used to determine σ^2 .

$$\underbrace{\begin{bmatrix} r(1) \\ \vdots \\ r(n) \end{bmatrix}}_{\equiv r_n} + \underbrace{\begin{bmatrix} r(0) & \dots & r(-n+1) \\ \vdots & \ddots & \vdots \\ r(n-1) & \dots & r(0) \end{bmatrix}}_{\equiv R_n} \underbrace{\begin{bmatrix} a_1 \\ \vdots \\ a_n \end{bmatrix}}_{\equiv \theta} = \begin{bmatrix} 0 \\ \vdots \\ 0 \end{bmatrix} \tag{29}$$

Such that $r_n + R_n \theta = 0$; where θ is the predicted coefficient and σ^2 is power estimate.

2.0 METHODOLOGY

The equipment used include; a multi-mode fibre cable (of about 59 meters), a patch panel, and Φ -OTDR (Anritsu MT9083AI Access Meter). The two basic types of pigtail available are; white/yellow (single-mode) and orange (multi-mode).

2.1 Patch Panel

This includes a patch cord, 22 port I/O interface, alcohol and connectors. A multi-mode fibre cable of about 50m is spliced to a patch cord of about 10m for the purpose of this study as shown in Plate 2.1. A fusion splicing machine is used to splice both cable and cord into a single measurement cable. A well spliced fibre cable reduces the reflection loss at the splice joints. A 22 port information outlet (I/O) interface connector is used for connectivity. The patch cord connects switches to the fibre cable.

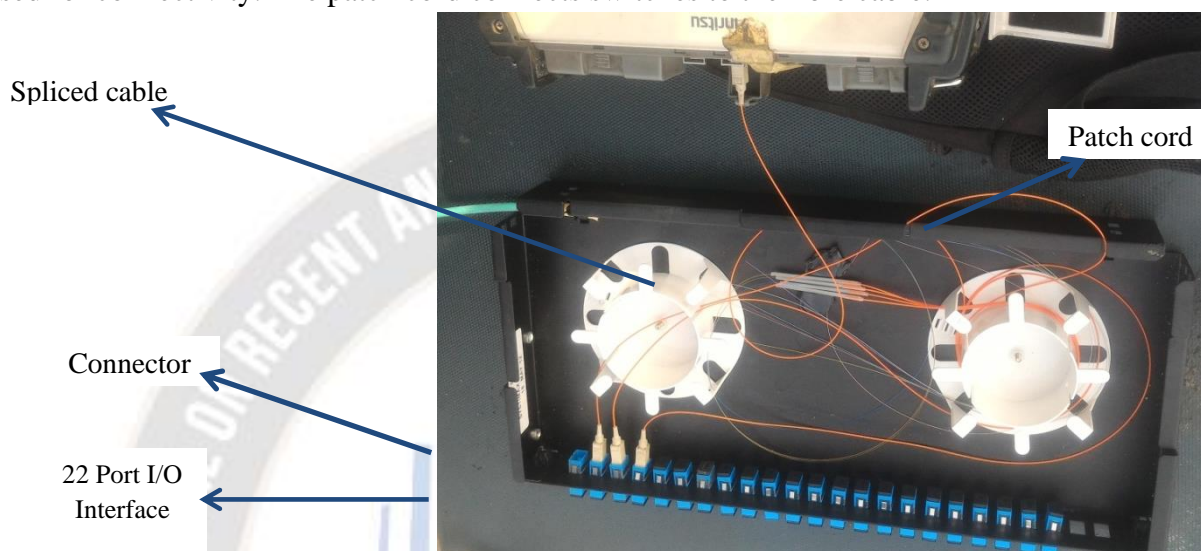


Plate 2.1: Patch Panel

During measurement, it was observed that continuous vehicular movement resulted to Fresnel reflection. The connector at the OTDR end was constantly cleaned, to prevent excess reflectance on the trace.

2.2 OTDR



Figure 2.1: OTDR ports

The top of the device comprises of the following ports; power meter, visual fault locator (VFL), OTDR, DC 12V, USB and Micro USB. Although, the OTDR has an in-built power meter, which is used to transmit light pulse into the fibre cable, some engineers prefer an external power meter to achieve same purpose. The VFL

is used to detect visually a defect within the cable. The DC 12V adapter is connected to the port to power the device and charge the battery. USB is used to copy measured traces from the internal memory and transferred to other devices.



Figure 2.2: OTDR model

The OTDR comprises of power button, which is switched on when used and off when measurement is completed. The navigation button controls the movement of the cursor/pointer, which the function button shows the various settings on the display screen as shown in Figure 2.2. The escape button returns the screen to the previous display screen. When the OTDR measurement is taken, the A-B button helps to navigate the trace. It is also used to calculate the attenuation of the trace from point A to point B. The OTDR button navigates the display to shows the previously measured trace in the internal memory of the device.

Before measurement is taken, the following information was keyed into the device; the length of the fibre cable, the pulse width used, measurement time, the deadzone is switched on and the wavelength is considered. For the purpose of this work, wavelength of 1300nm was used, with a pulse width of 10ns, distance range of 1km and a measurement time of 5seconds. If the auto setup is clicked, the device automatically chooses the default information and runs the test measurement and produces a trace based on its settings. The trace may incur excess noise, which may be unreliable, hence the need to choose appropriately the parameters necessary for the desired test. The trace obtained from the test measurement saved thereof.

Data Acquisition and Analysis: The setup comprise of patch panel, fibre cable installed on the groove and Φ -OTDR device. A multi-mode fibre cable was attached to a patch panel and mounted across the groove at Oluku By-Pass Bridge. The assistance of the Federal Road Safety official was required to hold traffic during the installation of the equipment. The patch panel was connected to the OTDR about 25metres from the bridge. The fibre cable was firmly placed at the joints and clipped to the groove using insulated material to conceal the cable in other to eliminate any extra perturbation.

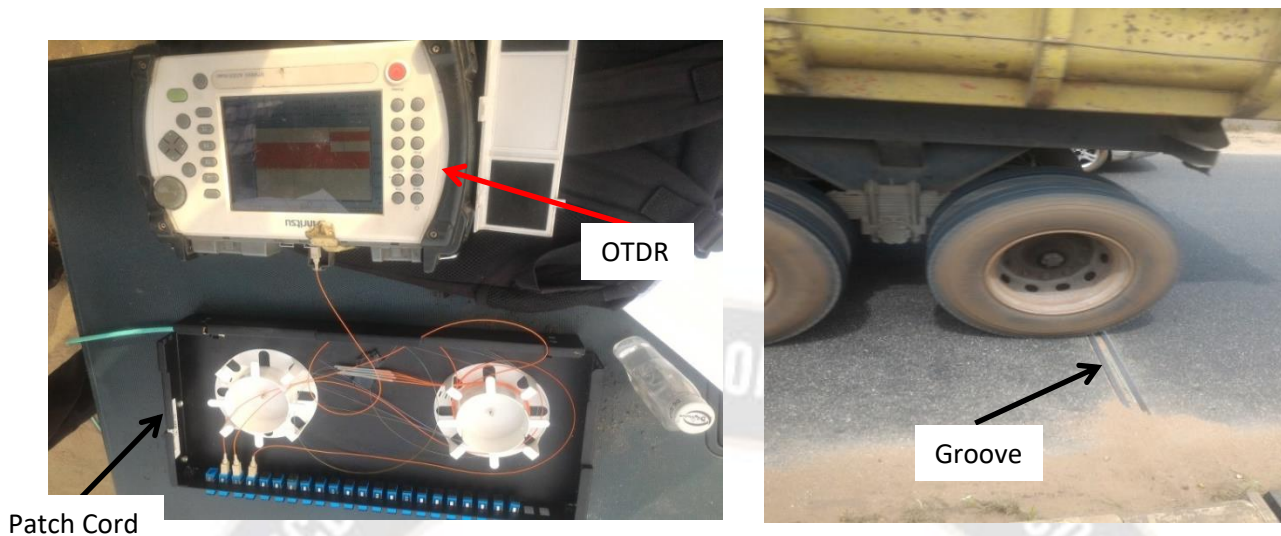


Plate 2.2: Experimental setup

A backscattering-based sensing technique was employed for a single-ended measurement with the OTDR. After installation, vehicular movement was allowed to continue. The effect of vibration caused by vehicular movement at distributed points of the fibre cable was measured using an Φ -OTDR at Oluku By-Pass Bridge. At same time, video shots were obtained to match the exact timing of the measured trace.

A 10ns pulse was sent into the fibre and records snapshots of stochastic signal caused by uncontrolled vehicular movement. Φ -OTDR measured the micro-bend between 26.16m - 58.57m, which is placed across the bridge and produces a trace as shown in Figure 2.4

When installing the equipment on the bridge, approximately 25m length cable was placed at the side of the bridge to the point of measurement for safety precaution. At about 25m, the cable was bent approximately 90° across the bridge within the groove. This resulted to the macrobend indicated on the trace, while the microbend was caused by the vibration induced by the uncontrolled vehicular movement. It also reports the refractive index of the core as 1.491; backscatter coefficient of -74dB and backscatter level along the cable caused by vehicular movement as shown in Figure 2.4

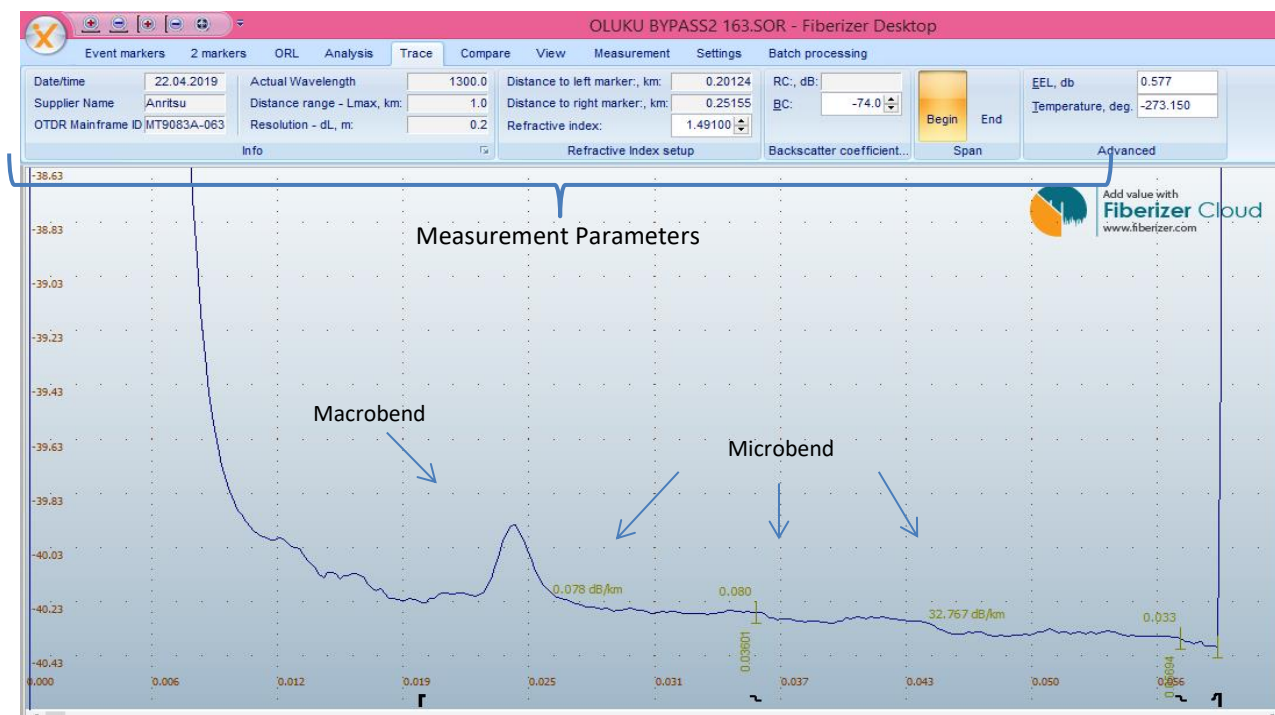


Figure 2.3: Fiberizer Cloud Trace

Each trace indicates the various measurement parameters. A trace records the date of test measurement, name of the OTDR, wavelength and so on as shown in Figure 2. The trace can be navigated by moving the two point marker (A and B). This is used to determine the loss between point A and B on the trace.

Sampled data is recorded approximately every 15 seconds. As light is sent through the fibre cable, the OTDR calculate the backscatter level along the fibre length as described in equation (11) and produce a trace. Several traces were recorded at 15 seconds time interval with video shots obtained to match the exact timing of the trace. The trace measurement identifies the notable events on the cable caused by the vehicle, which is analyzed to determine the vibration effect. When taking the trace, the vehicle incident on the cable, the timing of the trace and stochastic process were all considered. Video clips were also recorded to match the exact timing of each excitation. Data obtained from the OTDR is recorded and analyzed separately. The measured data obtained with FOS is further transformed from space domain to frequency domain using a Fast Fourier Transform (FFT).

It is impossible to determine the vibrating frequency of each vehicular movement, hence the need to analyze the spectra. It is observed that the signal has a wide range of frequency spectrum and impossible to determine the vibrating frequency of the signal. The covariance method as derived in equation (29) was considered due to its versatility (low frequency band) as shown in Figure 2.4

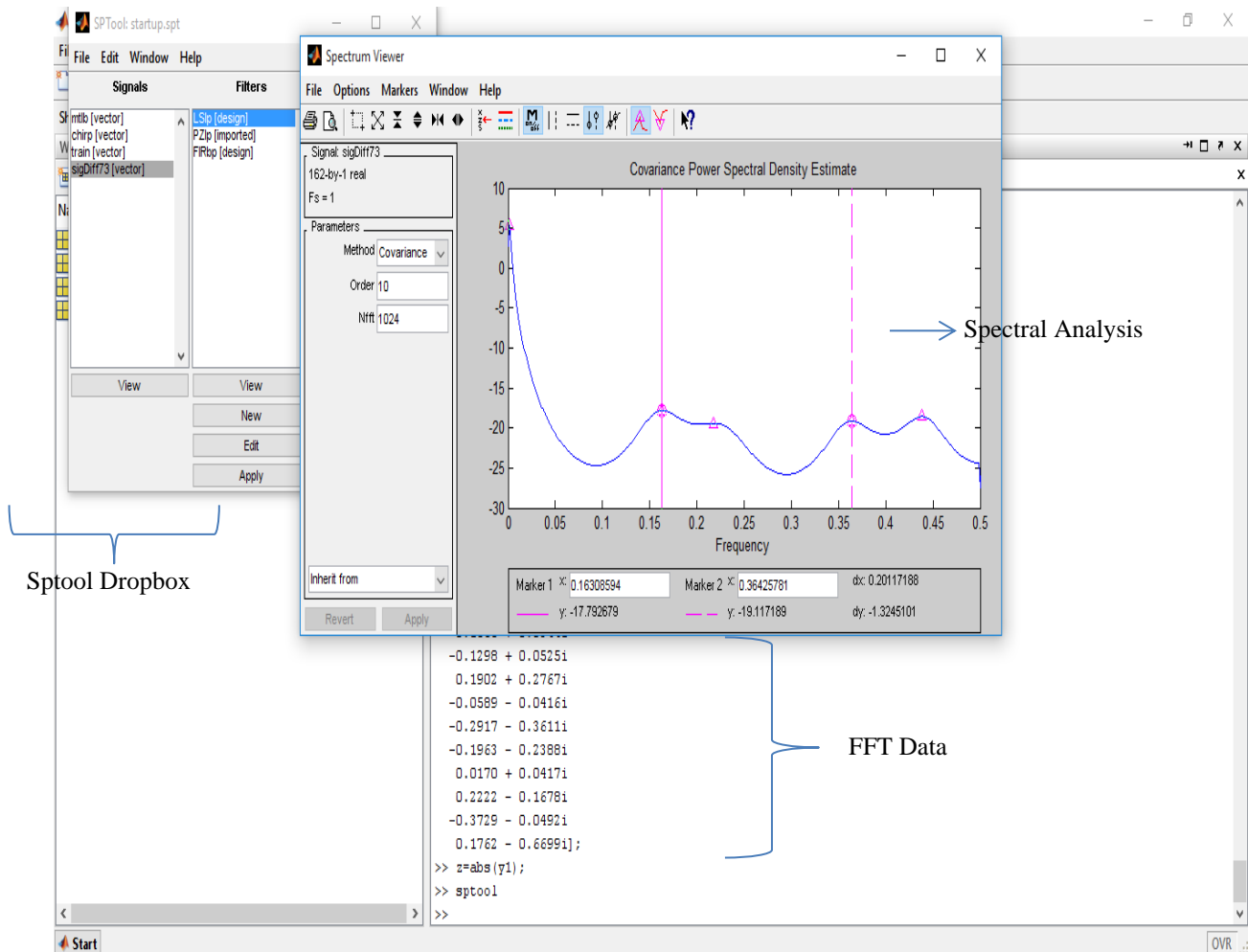


Figure 2.4: MATLAB window

Absolute value of the FFT data is determined by removing the first FFT value, which is extremely large. The purpose is to ascertain the exact frequency component of the signal. The absolute value is imported into the sptool dropbox in MATLAB 7.3 software. With noise embedded in the signal, a low band filter is used to eliminate the noise as shown in equation (24). In this work, a parametric model was used to calculate the spectral analysis of the uncontrolled vehicular movement. It was also observed that the choice of what order to use was also complex. The higher the order, the signal tends to display more peaks which represent noise. Conversely, at low order, the frequency peaks were characterized as a broad range of frequency. To this end, appropriate steps were taken to determine the exact filter to use to analyze the various spectra for the corresponding classes of vehicles used.

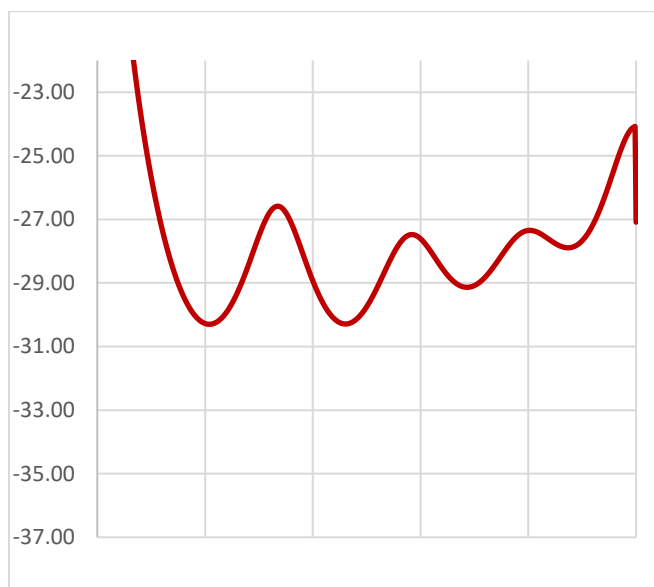


Figure 2.5(a): No Vehicles

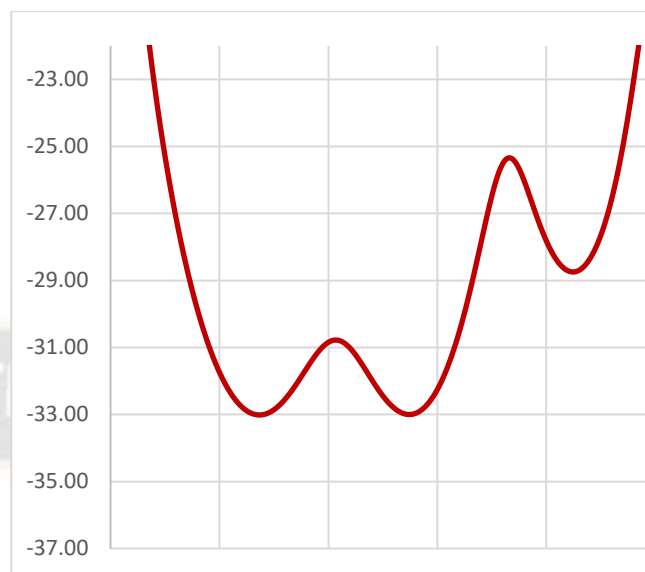


Figure 2.5(b): Cars and SUV

Figure 2.5(a) shows no vehicular movement within seconds of the trace. With no traffic recorded, it is expected that the excitation would be relatively calm but this was not so. According to Batenko *et al.*, (2011), excitation is measured with an OTDR as a vehicle approaches the sensing fibre at high speed less than 2 seconds from the trace. Hence, a very low excitation was recorded and shows a slight increase in the spectra. Curve 1 show peak of 2.1×10^{-3} dB with SD of 0.542 and curve 2 with peak of 1.9×10^{-3} dB with SD of 1.273 and curve 3 having a peak of 1.8×10^{-3} Hz with SD of 0.428. It is observed that curve 2 had a slightly higher peak with a high SD of 1.273 compared to 1.037 for Trace 79. Whereas, Figure 2.6(b) which recorded a few cars to have crossed the fibre within seconds of the trace showed 2 peaks. Curve 1 of Trace 79 show peaks of 0.9×10^{-3} dB with SD of 0.857 and 1.5×10^{-3} dB with SD of 1.037. It is observed that curve 2 which had the highest peak for Trace 79 with a high SD of 1.037 compared to 0.689 for the previous trace. This is probably due to excitation caused by 3 cars within 13 seconds of the trace.



Figure 2.6(a): 6 axle truck

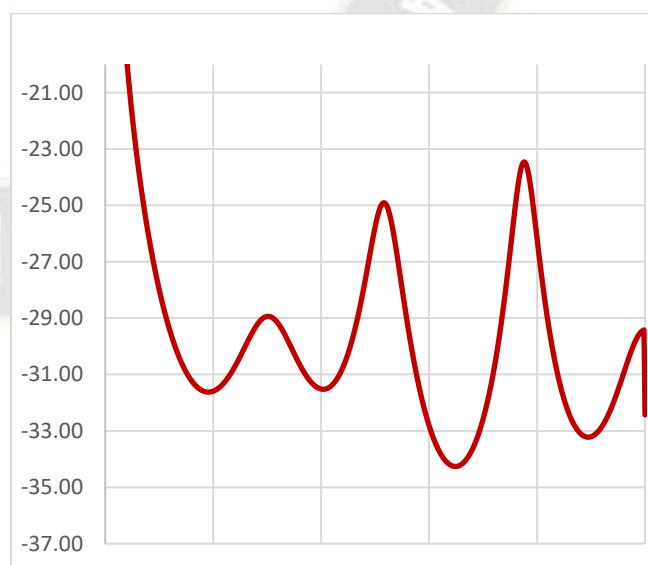


Figure 2.6(b): 5 axle truck

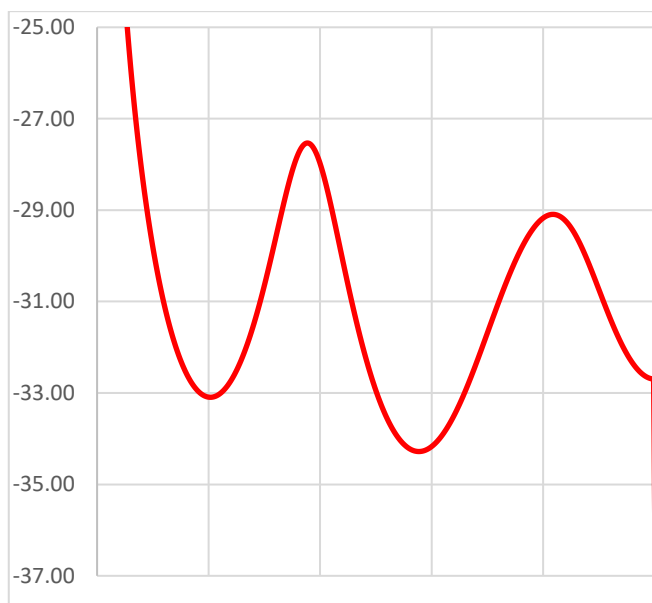


Figure 2.6(c): 4 and 3-axle truck

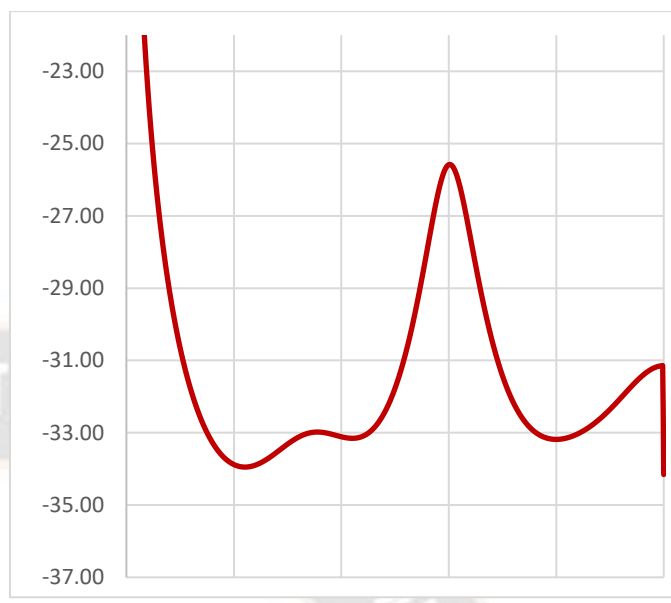


Figure 2.6(d): 3-axle truck

Figure 2.6(a) showed low traffic, which consist of cars and 6-axle truck within seconds of the Trace. The 6-axle truck at low speed tends to overshadow that of the low tonnage vehicles as shown above. This gives rise to 2 peaks of 3.3×10^{-3} dB with SD of 0.471 and 4.5×10^{-3} dB with SD of 0.650. It is observed that curve 2 had the highest peak with a higher SD of 0.650. Though the weight of the truck is expected to determine the width of each peak, this is not so because the OTDR measured the partial weight of the 6-axle truck crossing the fibre.

Figure 2.6(b) shows low traffic of vehicles within seconds of Trace at both low and high speed. The continuous excitation of the fibre at high speed gives rise to 3 peaks was obtained resulting in a 5-axle truck, which crossed the fibre. The spectra show curve 1 with peak of 1.3×10^{-3} dB with SD of 0.603, curve 2 with 3.1×10^{-3} dB with SD of 0.510 and curve 3 with peak of 4.5×10^{-3} dB with SD of 0.425. It is observed that the curve 3 had the highest peak with SD of 0.425, which is the same when compared curve 2 of the previous Trace. The increased excitation is probably due to high tonnage truck.

Figure 2.6(c) shows recorded 4 and 3-axle trucks within seconds of Trace at low speed. The resulting spectra indicate low peaks of 1.9×10^{-3} dB for curve 1 and 1.3×10^{-3} dB for curve 2 with SD of 0.599 and 0.148 respectively. It was observed that curve 2 had the lowest peak with SD of 0.148 compared to 0.769 of curve 2 from the previous Trace. This probably indicates that the truck was empty.

Figure 2.6(d) shows indicates low traffic consisting mainly of a car and a fully loaded 3-axle truck containing gravel crossed within seconds of Trace. The continuous excitations resulted in a single peak of 2.8×10^{-3} dB with SD of 0.477. Although the trace was recorded with seconds of the previous Trace, the peak is higher peak at a reduced SD, which is probably due to the excitation of the fibre caused to the high tonnage.

The various vibrating frequencies created by the different classes of vehicles identified by their tonnage can were further distinguished by their frequency widths and peaks using the full width at half maximum.

Description of spectral peaks with Full Width at Half Maximum (FWHM): The Gaussian distribution is introduced to describe the nature of each spectral peak by its Full Width at Half Maximum (FWHM). It is applied in many areas of science and engineering for this purpose. The FWHM is used to characterize a normal density curve by its standard deviation, c , through equation (4.1) (Leo, 2003).

$$FWHM = 2 c \sqrt{2 \ln 2} \cong 2.355 c \tag{30}$$

A double Gaussian is used in this work and gave a more precise fitting compared to a single Gaussian. It uses a sharp peak to characterize the waveform with a low root mean square error (RMSE) obtained from Figure . The statistics is presented in Table 4.

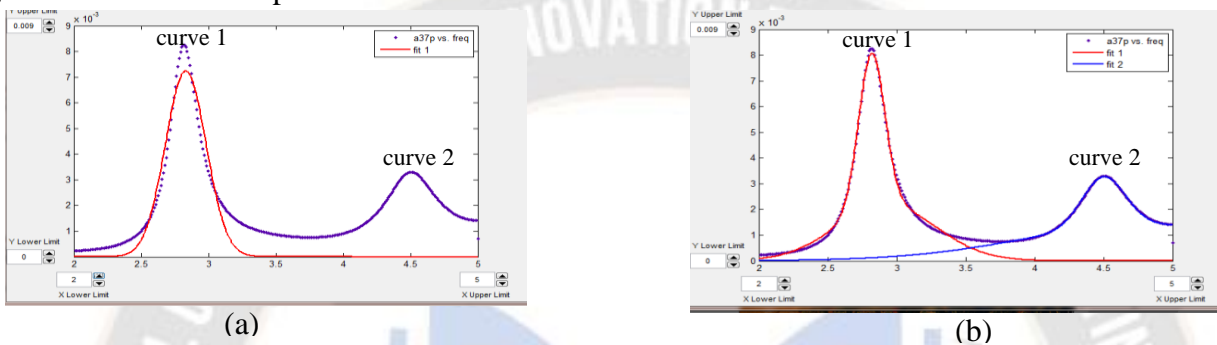


Figure 2.7 Gaussian fits to the spectra of Trace 37. (a) Single Gaussian fit. (b) Double Gaussian fit.

Table 2.1 Statistics of a double Gaussian fit to Figure 2.7

General model Gauss2: Curve 1	General model Gauss2: Curve 2
$f(x) = a1 * \exp(-((x-b1)/c1)^2) + a2 * \exp(-((x-b2)/c2)^2)$	$f(x) = a1 * \exp(-((x-b1)/c1)^2) + a2 * \exp(-((x-b2)/c2)^2)$
Coefficients (with 95% confidence bounds): a1 = 0.005966 (0.005838, 0.006094) b1 = 2.819 (2.817, 2.821) c1 = 0.1336 (0.1302, 0.1369) a2 = 0.002186 (0.002071, 0.002301) b2 = 2.922 (2.908, 2.937) c2 = 0.5094 (0.4845, 0.5343)	Coefficients (with 95% confidence bounds): a1 = 0.001949 (0.001895, 0.002004) b1 = 4.5 (4.497, 4.503) c1 = 0.222 (0.2165, 0.2276) a2 = 0.001401 (0.001307, 0.001495) b2 = 4.82 (4.709, 4.932) c2 = 1.261 (1.146, 1.376)
Goodness of fit: SSE: 1.8e-006 R-square: 0.9967 Adjusted R-square: 0.9965 RMSE: 0.0001369	Goodness of fit: SSE: 6.251e-008 R-square: 0.9993 Adjusted R-square: 0.9992 RMSE: 2.552e-005

Following this same procedure c_i or standard deviation, (SD), as a proxy for FWHM for all the respective curves in Traces 37 through 105 were calculated and presented in Table 4.

Table 2.2: FWHM analyses for various traces

Trace	Curve 1				Curve 2				Curve 3			
	c ₁	c ₂	Peak dB 10 ⁻³	RMSE ₁ x 10 ⁻⁵	c ₁	c ₂	Peak dB 10 ⁻³	RMSE ₂ x 10 ⁻⁵	c ₁	c ₂	Peak dB 10 ⁻³	RMSE ₃ x 10 ⁻⁵
37	0.134	0.509	8.00	13.69	0.222	1.261	3.20	2.55				
38	0.226	0.881	4.20	2.95	0.161	0.689	7.90	11.98	0.213	0.756	4.80	4.29
39	0.330	0.527	1.10	8.26	0.149	0.596	3.30	4.04	0.117	0.433	3.60	5.58
40	0.111	0.438	6.20	9.72	0.150	0.634	4.10	5.58				
71	0.138	0.471	3.30	4.72	0.202	0.650	4.50	4.98				
72	0.015	0.583	1.20	6.41	0.179	0.769	3.20	3.15				
73	0.141	0.599	1.90	4.72	0.623	0.148	1.30	2.29				
74	0.224	0.477	2.80	8.45								
76	0.198	0.713	2.70	2.10	0.191	0.705	2.50	3.53				
77	0.057	0.603	1.30	5.73	0.151	0.510	3.10	2.90	0.122	0.425	4.50	6.97
78	0.197	0.964	2.90	3.45	0.173	0.551	1.10	3.22	0.122	0.423	4.20	5.19
79	0.282	0.857	0.90	2.79	0.257	1.037	1.50	4.41				
80	0.061	0.542	2.10	9.30	0.304	1.273	1.90	5.05	0.852	0.045	1.80	6.26
81	0.130	0.425	5.00	4.79	0.159	0.493	3.90	2.49				
91	0.155	0.573	6.20	6.45	0.114	0.423	7.10	9.99	0.126	0.428	3.90	5.46
103	0.155	0.537	4.80	4.28	0.165	0.536	1.10	5.41				
104	0.533	0.428	1.00	4.86	0.057	0.190	9.40	24.40				
105	0.096	0.368	9.50	20.76	0.219	1.197	4.00	4.80	0.120	0.380	9.30	6.08

Note that the peaks of all coloured traces exceeded 4.0×10^{-3} dB, signifying excitations from either heavy duty trucks or vehicles at high speed.

With each consecutive trace recorded approximately 12-15 seconds with a pulse width of 10ns, it was observed that continuous excitation of the fibre cable at various speeds and vehicular traffic can be distinguished using this technique. It was observed from the study that high tonnage vehicles had sharp peaks and narrow standard deviation dependent on the axle type of the trucks. Also, snapshots of trace 105 recorded a combination of a 2-axle truck and 4 private vehicles (SUV and Bus) moving at high speed which indicated the three peaks of 9.50, 4.0 and 9.30×10^{-3} dB. Furthermore, cars at high speed and low traffic give a standard deviation above 0.6, whereas, low tonnage cars at low speed and high traffic give a standard deviation less than 0.6 at low traffic. The results from WIM can be used to identify heavy trucks and over speeding of cars on the highway. It is observed that high tonnage vehicles give a high frequency peak with narrow width which represent the highlighted peaks are traces in Table 2.2. Whereas, the low frequency peaks were caused by low tonnage vehicles at both low and high speed. To this end, special attention should be made towards heavy duty trucks in order to avoid rampant road failure within the country. Reckless driving can be checkmated on the highway, which can reduce frequent accidents.

3.0 CONCLUSION

A distributed fibre optic vibration sensor is used to measure stochastic signal caused by vehicular movements at Oluku Bypass Bridge. The vehicular traffic was uncontrolled, in other to ascertain the random

nature of the signal and calculate the spectral analysis. The installation of the cable was successful, with the fibre cable placed inside the groove and buried with sand. Although it took several vehicular movements to excavate the sand from its position but at each point, the cable was reburied. The tensile strength of the fibre cable was able to withstand a large amount of depression caused by the vehicles when the cable did eventually escape from the groove. The 10ns light pulse from the Φ -OTDR is sufficient to take milliseconds snapshot of the stochastic process caused by vehicular movement. Also, the spectra of the measured data were calculated to identify peaks at various frequencies of the vibrating signal, which indicate different frequencies of vibration of the stochastic signal. The spectra exhibited sharp frequency peaks for high tonnage vehicles. The frequency distribution for both high and low tonnage vehicles were analyzed using the FWHM. Similarly, the result was used to classify the vehicles by identifying the FWHM obtained with double Gaussian model for differential trace indicate high traffic gives sharp peaks with standard deviation less than 0.6 and above 0.6 for low traffic. Finally, the analyses showed peaks above 4.0×10^{-3} dB for traces with trucks and cars at high speed, while peaks less than 4.0×10^{-3} dB were obtained for traces with cars. In conclusion, although Φ -OTDR is strictly used for communication, this study has identified the diversity of the equipment in fibre optic sensor measurements (in structural health monitoring and pipeline leakage).

4.0 RECOMMENDATION

Further research should be done to emphasize on the following:

1. The FWHM shows traffic consisting mostly of trucks and a combination of trucks gives sharp peaks above 4.0×10^{-3} dB and 7.0×10^{-3} dB respectively at low and high speed.
2. The FWHM shows that traffic which consist mostly of trucks and a combination of trucks and cars gives sharp peaks with SD less than 0.450 at high speed. Also, cars at high speed give a standard deviation above 0.6, whereas, cars at low speed give a standard deviation less than 0.6 at low traffic.
3. Spectral analysis should be considered for controlled vehicular movement at different speed and weight using this technique.
4. The technique can be employed to obtain the frequency of vibration on the lattice structure of a wind turbine and detect specific location of pipeline leakage.
5. The technique can also be used in structural health monitoring and monitor vehicular movement to characterize the vehicle tonnage.

REFERENCES

1. Zang Xiao-Yan (2007): The Adjustment of Vibration sensors and the analysis of error margin; Journal of Shandong, Institute of Commerce and Technology, 7(6); 102-106.
2. Xuji (2010): Choice and Installation of the vibration transducer; Journal of Metrology and measurement technique, (1); 45-46.
3. Awodu O.M., Ukagwu K.J., Okuonghae T., Andikara J.N. and Azi S.O. (2019): Vibration measurement of vehicular traffic at Oluku by Pass Bridge using Fibre Optic Sensor. *Indian Journal of Engineering*, vol.16, pp. 342-347
4. Malla R. B., Sen A., and Garrick N. W. (2008): A Special Fibre Optic Sensor for Measuring Wheel Loads of Vehicles on Highways; Multidisciplinary Digital Publishing Institute. ISSN 1424-8220, Sensors 8; 255-2568
5. Agrawal, Govind (2010), *Fibre Optic Communication Systems (4 ed.)*, Wiley, doi: 10.1002/9780470918524, ISBN 978-0-470-50511-3
6. Gholamzadeh, B., and Nabovati, H. (2008): Fibre Optic Sensors, Proceedings of World Academy of Science, Engineering and Technology, Vol. 32, pp. 303 – 313 (2008).
7. Patra, T. (2013): A Simple Fibre Optic Displacement Sensor for Measurement of Light Intensity with the Displacement, International Journal of Latest Trends in Engineering and Technology (IJLTET), Vol. 2 Issue 1 (2013).

8. Nurulain S., Mazlee N.N., Salim M. R. and Manap H. (2017): A review on Fibre optic sensor Topology and Modulation Technique; International Journal of Engineering Technology and Sciences, vol. 7(1).
9. Ginu R. (2015): Optical Fibre Sensor (Advanced Techniques and Applications); CRC Press, Taylor and Francis Group, 6000 Broken Sound Parkway NW, suite 300, Boca Raton, FL 33487-2742. ISBN-13: 978-1-4822-2829-8. pp 1-12.
10. Hisham K.H. (2018): Review Article; Fibre optics Sensing Technology: basics, classifications and applications; American Journal of Remote Sensing. ISSN: 2328-5788 (print); ISSN: 2328-580X (Online). Vol. 6(1), Pg 1-5.
11. Adewuyi A.P., Wu, Z. and Serker N.K. (2009): Assessment of vibration-based damage identification methods using displacement and distributed strain measurements, Structural Health Monitoring volume 8, 443–461
12. Sheng-he (2009): Development trend of modern sensor; Journal of Electronic Measurement and Instrument, 23(1); 1-10
13. Minsili and Xia (2010): Application of Time Delay Consideration on Bridge Vibration Control Method with Active Tendons; Leonardo Electronic Journal of Practices and Technologies. ISSN 1583-1078; Issue 16, January-June 2010, 101-118
14. Liu Y., Liua X., Maa C and Zhou Y. (2018): Micro-structured optical fibre sensor for simultaneous measurement of temperature and refractive index: Optical Fibre Technology; vol. 41, 168–172
15. Kumar P., Chandrasekaran N. and Garg M. (2014): Fibre Optic Sensor for Localized Vibration Measurement; Fibre Optics Lab, Institute of Armament Technology, India -411 025.
16. Palmieri L. and Schenato L. 2013: Distributed Optical Fibre Sensing Based on Rayleigh Scattering; The Open Optics Journal, volume 7, (suppl-1, M7), pp 104-127
17. Zhang Z. and Bao X. (2008): Distributed optical fibre vibration sensor based on spectrum analysis of Polarization- Φ -OTDR system; Optical Express 10240 Vol 16(14)
18. Wang Q., Han L., Fan X. and Zhu J. (2018): Distributed fibre optic vibration sensor based on polarization fading model for gas pipeline leakage testing experiment; Journal of low frequency, noise, vibration and active control. Vol. 37(3), pp. 468-478
19. Yang M., Li S. and Jiang D. (2014): Review on Fibre optics Sensing Technologies for Industrial Applications at NEL-FOST; 7th European Workshop on Structural Health Monitoring. July 8-11, La Cite, Nantes, France.
20. Semenova Y. and Farrell G. (2015): Optical Fibre Sensor (Advanced Techniques and Applications); CRC Press, Taylor and Francis Group, 6000 Broken Sound Parkway NW, suite 300, Boca Raton, FL 33487-2742. ISBN-13: 978-1-4822-2829-8. pp 13-32.
21. Batenko A., Grakovski A., Kabashkin I., Petersons E., Sikerzhicki Y. (2011): Problems of Fibre Optic Sensor Application in Weight-in-Motion (WIM) Systems; The 11th International Conference “Reliability and Statistics in Transportation and Communication. (RelStat’11), 19–22 October 2011, Riga, Latvia, p. 311-316. ISBN: 978-9984-818-46-7. Transport and Telecommunication Institute, Lomonosova 1, LV-1019, Riga, Latvia
22. Crickmore R. I. and Hill D. J. (2010): Traffic sensing and monitoring apparatus. US7652245B2.
23. Hartog, A. H. (2017): Introduction to Distributed Optical Fibre Sensor; Series in Fibre Optic Sensor. Taylor and Francis Group, 6000 Broken Sound Parkway NW, Suite 300 Boca Raton, FL 33487-2742. CRC Press
24. Zhao H., Wu D., Zeng M., and Zhong S. (2018): A Vibration-Based Vehicle Classification System using Distributed Optical Sensing Technology; Transportation Research Record 1–12: National Academy of Sciences: Transportation Research Board 2018 Reprints and permissions: DOI: 10.1177/0361198118775840. journals.sagepub.com/home/trr
25. Schulz W. L., Conte J. P. and Udd E. (2001): Long-gage fibre optic Bragg grating strain sensors to monitor civil structures, 8th Annual International Symposium on Smart Structures and Materials, Newport Beach, CA, USA, SPIE: 56–65.
26. Liu X., Jin B., Bai Q., Wang Y., Wang D. and Wang Y. (2016): Review on Distributed Fibre-Optic Sensors For Vibration Detection; doi:10.3390/s16081164. Multidisciplinary Digital Publishing Institute. Sensors 16, 1164
27. The Fibre Optic Association. Retrieved April 17, 2015, <http://www.thefoa.org/tech/ref/testing/Φ-OTDR/Φ-OTDR.html> ;
28. Sifta R., Munster P., Sysel P., Horvath T., Novotny V., Krajsa O. and Filka M. (2015): Distributed fibre-optic sensor for detection and localization of acoustic vibrations; Metrology and Measurement Systems 22(1), 111-118
29. Ren M. (2016): A Thesis on ‘Distributed Fibre Optic Sensor Based on Phase-Sensitive OTDR’, Faculty of Graduate and Postdoctoral Studies, University of Ottawa, Ottawa, Canada
30. Qin Z. (2013): A Thesis on ‘Distributed Fibre Optic Vibration Sensor Based on Rayleigh Backscattering’, Faculty of Graduate and Postdoctoral Studies, University of Ottawa, Ottawa, Canada.
31. Awodu O.M., Ukagwu K.J., Azi S.O. and Babalola M. (2019): Optical Fibre Sensor (Theory and Experiment); African Multi-Disciplinary Journal, Kampala International University, Uganda.
32. Lujo I. and Klokoc P. (2008): Fibre-Optic Vibration Sensor Based on Multi-mode Fibre; Journal of Radio Engineering, 17(2), 93-97.

33. Bayat M. and Abdollahi H. (2016): Various Types of Parametric Methods of Power Spectral Density Estimation; International Journal of Megatronics, Electrical and Computer Technology. Vol. 6(19), pp. 2719-2735. IJMEC DOI: 649123/10189.

